

Immiscible lipids control the morphology of patchy emulsions†

Cite this: *Soft Matter*, 2013, **9**, 7150

Lea-Laetitia Pontani,* Martin F. Haase, Izabela Raczkowska and Jasna Brujic*

We study the phase behavior of immiscible mixtures of phospholipids and cholesterol at the interface of oil-in-water emulsions, which governs the surface morphology of patchy droplets. Emulsification with lipid mixtures leads to domain formation with a variety of shapes, such as spots, disordered stripes, hemispheres and rings. We map out the ternary immiscibility diagram of our system, which allows one to control the geometry of patches on the droplet surface. By contrast to short-lived domains on liposomes, image analysis of the individual domains shows that emulsion spots grow towards a steady state size distribution and remain stable over weeks. These domains are functionalized with biotinylated lipids, which makes them useful candidates for directed self-assembly through specific interactions *via* streptavidin. Here we bind streptavidin coated beads to these lipids and find that the binder diffusion constant depends on the morphology of the droplet. These fluid patchy particles offer a versatile system in which the geometry and the dynamics of the sticky patches are under control.

Received 24th April 2013

Accepted 6th June 2013

DOI: 10.1039/c3sm51137e

www.rsc.org/softmatter

1 Introduction

Much progress has been made in recent years in understanding the mechanisms of self-assembly of building blocks on different length scales.¹ Biological systems employ principles of directed association of individual components to perform particular functions, while physical systems are designed to build complex superstructures with tunable optical,^{2–4} mechanical^{5,6} and electronic properties.^{7–9} In order to achieve particular structures, constituent particles are designed to have anisotropic features through which they can specifically interact.^{10,11} Depending on the anisotropy of the particle, numerical simulations predict a variety of macroscopic architectures, such as sheets, chains, controlled clusters and rings.^{10–12} Experimentally, the anisotropy of the particle can be induced by chemical patterning with gold nanoparticles,¹³ functionalization of sticky patches fixed on the surface,^{14,15} permanent dipoles^{16–18} and shape control in the case of cubic¹⁹ or dimpled colloids.²⁰ All these techniques involve multi-step chemical procedures and result in solid particles in which the anisotropy is fixed once the particle is made.

Here we present a novel way to make anisotropic soft particles by a single-step synthesis of oil-in-water emulsions that are co-stabilized by ternary mixtures of phospholipids and cholesterol. More specifically, we use lipid mixtures of 1,2-dioleoyl-*sn*-glycero-3-phosphocholine (DOPC), brain sphingomyelin (BSM)

and cholesterol (Chol) that are close to the composition of the outer leaflet of biological membranes^{21,22} and are therefore useful tools to address the existence of sphingolipid/cholesterol-rich rafts in a simplified environment.^{23–29} These mixtures are known to form spontaneous coexisting liquid phases in membranes^{30–35} and in monolayers at the air–water interface.^{36–39} Here we exploit the fact that these lipid domains are much more stable in monolayers than in bilayers to make long-lived patches at the interface of oil-in-water emulsion droplets. The advantage of this system over solid functionalized particles is that the domains are free to move on the fluid emulsion interface and thus explore a broader spectrum of accessible architectures. Moreover, the miscibility phase diagram of the lipids determines the morphology of the droplets and the size distribution of the domains. Furthermore, the variability of the available phospholipids with functionalized hydrophilic heads allows one to tune the nature and strength of the interaction between neighboring droplets to facilitate their self-assembly through biologically active molecules. These interactions may include adhesive proteins, such as the biotin–streptavidin complex,⁴⁰ lock and key interactions with antibody–antigen recognition,^{41,42} complementary DNA strands^{43,44} or cellular adhesion proteins, such as cadherins.

2 Materials and methods

2.1 Polydisperse emulsion preparation

The protocol for the emulsion preparation is similar to the one described in ref. 40. The oil droplets are stabilized with mixtures of 1,2-dioleoyl-*sn*-glycero-3-phosphocholine (DOPC) and brain sphingomyelin (BSM) lipids and cholesterol in various

New York University, Department of Physics and Center for Soft Matter Research, 4 Washington Place, New York, United States. E-mail: jlb2929@nyu.edu; llp6@nyu.edu
† Electronic supplementary information (ESI) available. See DOI: 10.1039/c3sm51137e

stoichiometries, while the labeling of the surfaces is performed with 1,2-distearoyl-*sn*-glycero-3-phosphoethanolamine-*N*-[biotinyl(polyethylene glycol)-2000] (ammonium salt) (biotinylated lipid) or 1-myristoyl-2-[12-[(7-nitro-2-1,3-benzoxadiazol-4-yl)-amino]dodecanoyl]-*sn*-glycero-3-phosphocholine (NBD PC). The lipid products were purchased from Avanti Polar Lipids (Alabaster, AL). All other chemicals were purchased from Sigma-Aldrich. The molar ratios of DOPC, BSM and cholesterol are varied to explore the phase diagram while 4% of biotinylated lipids is introduced to label the phases with fluorescent streptavidin (Texas Red, Alexa Fluor 488 or Alexa Fluor 647 conjugated, purchased from Invitrogen). A 350 Cst silicone oil is saturated with the lipids that are introduced at a total mass of 20 mg mL⁻¹, before emulsification. The final emulsion is index matched in the buffer containing 1 mM SDS, 2 mM Tris-HCl, pH = 7.5, in a 50 : 50 glycerol-water solution, and kept at 4 °C. Samples of 100 μL of the emulsion are mixed with 5 μL of streptavidin at a concentration of 1 mg mL⁻¹ and 300 μL of the buffer solution. This solution is incubated for 1 h at 4 °C to allow the streptavidin to bind to the biotinylated lipids on the droplets. The sample is imaged using a fast scanning confocal microscope (Leica TCS SP5 II).

2.2 Monodisperse emulsion preparation

Monodisperse emulsions are produced with a microfluidic technique adapted from ref. 45. Since this method requires the use of capillaries with diameters as small as 15 μm, the viscosity of the oil is reduced to 50 Cst to ensure reasonable flow rates with the available syringe pumps. The oil preparation remains unchanged and the lipids are dissolved in it as described in the previous section. Round borosilicate glass capillaries (inner diameter ID = 0.4 mm, outer diameter 0.55 mm, Fiber Optic Center Inc.) are pulled in a micropipette puller to produce tip openings ranging from 15 to 60 μm. Two capillaries with different tip openings are then inserted into a larger square capillary (ID 0.6 mm). The smaller one is interdigitated into the larger one (see Fig. 2) before the set up is finally fixed onto a supporting glass slide with epoxy glue. The square capillary and the free end of the smaller round capillary are both connected to syringe pumps (NE-300, New Era Pump Systems). After flushing with ethanol in a clean environment, the set-up is transferred at 4 °C for the rest of the process. The continuous phase buffer (5 mM SDS and 2 mM Tris, pH = 7) is pumped into the square capillary at rates ranging from 500 to 2000 μL h⁻¹, while the lipid containing oil is pumped into the smallest capillary at rates from 10 to 40 μL h⁻¹. The oil droplets flow out of the larger round capillary with the larger tip diameter and are collected after creaming.

2.3 Image analysis

We analyse the 3D images of the transparent monodisperse emulsions to extract the positions and sizes of thousands of domains in the sample. The image is sharpened by filtering out the low frequency noise. This step ensures that the small individual domains are well separated. The Otsu thresholding algorithm⁴⁶ is then used to binarize the original image into white domains and a black background. The connected regions

in the binarized image are identified as domains with positions given by their centers of mass. The diameter of each domain is given by the length of the smallest cube that encloses the domain. This allows us to measure the evolution of the distribution of domain diameters as a function of time and lipid composition.

2.4 Diffusion coefficient measurement

We use 1 μm magnetic particles, coated with streptavidin (Dynabeads MyOne Streptavidin C1, Invitrogen), as reporters of the lipids diffusion on the surface. The emulsion droplets (5 μL of creamed emulsion) are incubated with the particles (1 μL) in a buffer containing 4 mM MgCl₂, 2 mM Tris, pH = 7.5, 1 mM SDS (600 μL) to allow the colloids to attach to the biotinylated lipids on the droplets surface. We then follow the motion of the bead on the surface of the droplets. The image is focused and centered on the bead diffusing on the bottom of the creamed athermal oil droplet and the movie is acquired at frame rates from 2.5 to 10 images per second. The position of the bead is obtained at each time by thresholding the image and isolating it from the immobile droplet. The mean square displacement of the bead confirms a diffuse behavior and the corresponding diffusion coefficients are obtained for various compositions.

3 Results and discussion

3.1 Lipid stabilized emulsions display a wide range of surface morphologies

Coarse emulsification of the droplets using an iso-stoichiometric mixture of DOPC-BSM-Chol leads to a variety of domain shapes and sizes, as shown in the 3D confocal image projection in Fig. 1a. This diversity may arise from the non-uniform composition of the lipids on the droplet surfaces during emulsification in the narrow gap couette cell. Similarly, small variations in the lipid composition were shown to induce

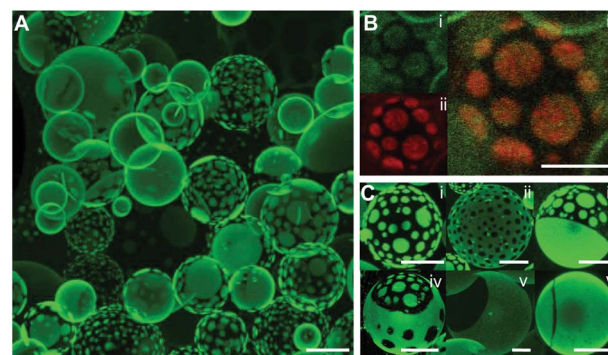


Fig. 1 (A) 3D projection of a polydisperse emulsion made with 19% DOPC, 77% cholesterol and 4% biotinylated lipids. The biotinylated lipids are labeled with fluorescent streptavidin and reveal the separation of the lipids into immiscible domains on the surface. (B) The fluorescent signal of the lipid NBD PC (i) labels liquid disordered phases in bilayers and here overlays with the fluorescent streptavidin signal in red (ii). The merged picture (iii) shows the colocalization in orange. (C) Different domains morphologies are identified within the same emulsion: (i) green spots; (ii) black spots; (iii) green spots/green cap; (iv) mixed spots; (v) Janus; (vi) ring. All scale bars = 5 μm.

large changes in the phase behavior of liposomes.⁴⁷ We identify a broad spectrum of available patterns, shown in Fig. 1c, including bright spots, dark spots, coexisting spots, Janus droplets, and rings. These patterns are independent of the radius of the droplet, indicating that curvature plays a negligible role on the colloidal length scale (see ESI†). In model membranes, these patterns are due to the liquid–liquid immiscibility of the species and are composed of two types of domains: the liquid ordered (L_o) and liquid disordered (L_d) phases.³⁰ The cholesterol and sphingomyelin are enriched in the L_o phase, while DOPC is concentrated in the L_d phase.⁴⁸ In our system, the bright regions are labeled with fluorescent streptavidin, which binds to the biotinylated lipids, but this measurement does not reveal the phase type. We therefore add another fluorescent probe, the lipid NBD-PC, which is known to enrich into the L_d domains of lipid bilayers.⁴⁹ In Fig. 1c, the colocalized fluorescence signals of the NBD-PC and the streptavidin show that the biotinylated lipids label the DOPC rich phase, which we use as the label throughout the article. In addition, replacing the biotinylated lipids with 4% of another labeling lipid, NBD-PC, does not affect the formation of domains when mixed with equal amounts (48%) of DOPC and cholesterol. This result suggests that the biotinylated lipids do not play a dominant role in the segregation of the species.

3.2 Immiscibility phase diagram of lipids in emulsions

To gain control over the domain morphology we produce monodisperse athermal emulsions using a flow-focusing microfluidic device, as shown in Fig. 2A and B.⁵⁰ For a given lipid composition, these droplets exhibit reproducible and homogeneous lipid patterns. For example, a binary mixture of DOPC–Chol (1 : 4) produces bright spots on a dark background

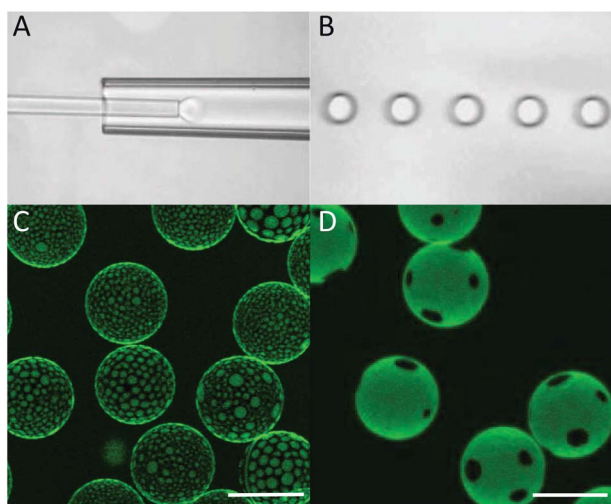


Fig. 2 Flow-focusing technique for the production of monodisperse emulsions. (A) A thin capillary (opening diameter $\sim 20 \mu\text{m}$) flows the lipid containing oil into a larger capillary in which the continuous phase is flown as well. This results here in the production of monodisperse droplets of diameter = $24 \mu\text{m}$ (B). Homogeneous morphologies are obtained throughout the obtained monodisperse emulsions. The patterns depend on the lipid composition, bright spots (C) are formed with a DOPC–cholesterol (1 : 4) ratio while dark spots (D) appear for an iso-stoichiometric mixture. Scale bars = $20 \mu\text{m}$.

in Fig. 2C. The morphology of the droplets does not depend on the droplet size in the range from 20 to $54 \mu\text{m}$ in diameter (see ESI†). Reducing the cholesterol level inverts the phases and gives rise to dark spots on a bright background, as shown in Fig. 2D. Interestingly, in this case there are on average six dark spots per particle, which would set the coordination number of an assembly of such particles, provided that the dark spots are functionalized with binders.

Next, we characterize the ternary immiscibility diagram for mixtures of DOPC–BSM–Chol lipids in monolayers formed at the oil-in-water emulsion interface. This circumvents the problem of DOPC oxidation that occurs at the air–water interface.^{51,52} Phase diagrams for similar lipid mixtures are described in terms of α and a β -region,⁵³ which correspond to different transition pressures at the apparition of domains.^{38,39} Instead, here we construct the phase diagram by characterizing the domain morphology as a function of the lipid composition following the methodology employed for patchy nanoparticles.⁵⁴ This classification is based on distinguishing droplets with bright or dark spots, stripes, gel structures and homogeneous surfaces, as shown by the legend in Fig. 3. Using this phase diagram one can produce droplets with the desired morphology by emulsifying at the corresponding lipid composition.

Just as in the case of monolayers at the air–water interface,^{38,39} the binary axis of DOPC–cholesterol in Fig. 3 reveals domain formation for cholesterol concentrations above 30%. Initially, the cholesterol-rich dark spots diffuse on a bright background of DOPC. Above 60% of cholesterol the phase inverts to form bright spots on a dark background. This inversion confirms the previous observation that cholesterol separates from the bright phase containing DOPC and the biotinylated lipids that colocalize with NBD-PC. The ternary phase diagram reveals that

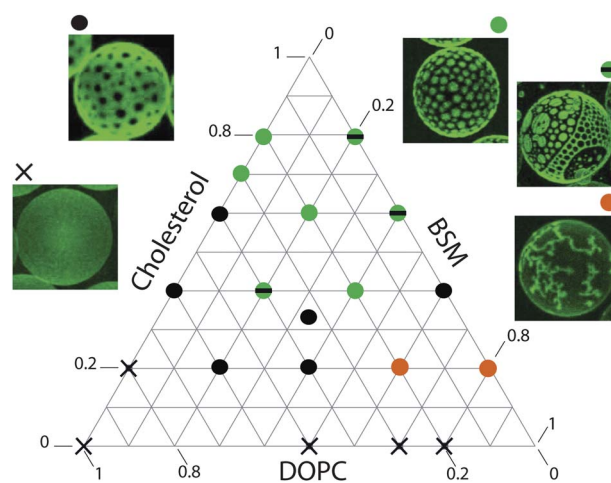


Fig. 3 Immiscibility diagram for ternary mixtures of DOPC–BSM–cholesterol stabilizing monodisperse emulsion droplets. This mixture constitutes 96% of the lipids on the surface since 4% is always dedicated to biotinylated lipids for fluorescent labeling. We report the steady state morphologies observed after times ranging from ~ 1 min to several hours. The patterns are classified into different categories: bright spots on a dark background (green circles); dark spots on a bright background (dark circles); bright tree-like structures on a lighter background (orange circles); mixtures of bright and dark spots (green circle with a black line); homogeneous surface (crosses).

regions between dark and bright spots are populated with emulsions that exhibit coexisting patterns of the two phases, as shown for example by the point at (DOPC–BSM–cholesterol; 40 : 20 : 40). Owing to the high melting temperature of BSM ($T_m = 50\text{ }^\circ\text{C}$), increasing its concentration leads to the precipitation of these lipids into a solid phase, which form fluorescent branched patterns on the droplet surfaces. These branches float on the surface as rigid bodies without the shape fluctuations observed for the liquid–liquid coexistence regions.

3.3 Domain formation and stability

While the phase diagram in Fig. 3 is based on the final state observed for each composition, here we investigate the kinetics of domain formation and their stability. At room temperature, the domain topology on the surface of a droplet evolves on a time scale that depends on the lipid mixture. Minutes after heating emulsions containing large amounts of cholesterol from $4\text{ }^\circ\text{C}$ to room temperature we observe the formation of disordered stripes, as shown in Fig. 4A for the mixture DOPC–Chol (1 : 4). These stripes then coarsen into stable bright spots shown in Fig. 4B. Following a single droplet over time reveals that the low viscosity bright phase extends fingers with increasing thickness into the higher viscosity dark phase over an hour, as shown in the snapshots in Fig. 4C. These fingers then evolve into bright spots on a dark background, as shown for the example droplet in Fig. 4D. While all droplets achieve the bright spot pattern in the time frame of 24 hours, the variability in this timescale between individual droplets spans from the onset of imaging (*i.e.* minutes) to hours.

The observed mechanisms of domain formation are reminiscent of viscous fingering into disordered stripes and spinodal decomposition into spots in liposomes,³³ or more broadly in

coexisting liquid phases in 2D systems.^{55,56} However, these processes are much faster in liposomes and take place on the timescale of seconds. The final segregated domain shapes have been observed and explained in coexisting liquid phases in monolayers, either as kinetic traps along the way to phase separation,⁵⁷ or as equilibrium patterns at the air–water interface.⁵⁸

In order to determine whether the patches formed on the droplets are at equilibrium we next investigate their evolution over long times. We observe that the domains slowly ripen on the timescale of hours through coalescence, as shown in the sequence in Fig. 5A. In each image, the arrow points to the domain that coalesces with a neighboring domain in the subsequent image. To quantify this effect in a statistically significant manner, we image a 3D packing of patterned emulsion droplets that cream under gravity, as shown in Fig. 5B. Image analysis methods are then employed to identify the position and diameter of each circular domain, as shown by their superposition with the original image in Fig. 5C. After the initial nucleation of domains, which are below the resolution of the image analysis method, their average diameter only grows by 25% over two weeks, as shown in the graph in Fig. 5D. This result suggests that the domains are stable on experimental timescales and may imply equilibrium conditions. It is also interesting to note that the size distribution of domains is non-Gaussian and has a broad tail of large domains, as shown in the inset in Fig. 5D. Such a stability for lipid domains is only observed at air–water interfaces,^{58,59} where the equilibrium shape and stability are controlled by the balance of line tension and electrostatics. The line tension arising from the segregation of the lipids drives fusion of the domains into a Janus particle to

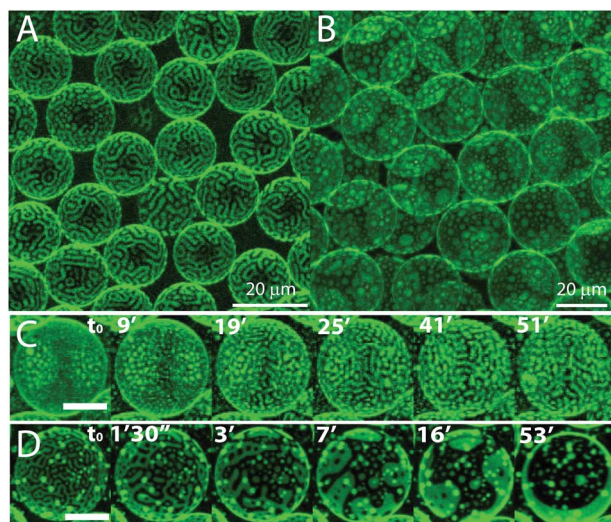


Fig. 4 A large number of droplets with homogeneous patterns can be packed together and imaged in 3D. The same mixture (DOPC–cholesterol 1 : 4) first reveals disordered stripes (A), before displaying bright spots on all the droplets (B). The formation of disordered stripes appears right after heating up to room temperature and looks similar to viscous fingering (C), and is followed by the formation of spots that takes also ~ 1 hour (D). Scale bars = $10\text{ }\mu\text{m}$ in (C) and (D).

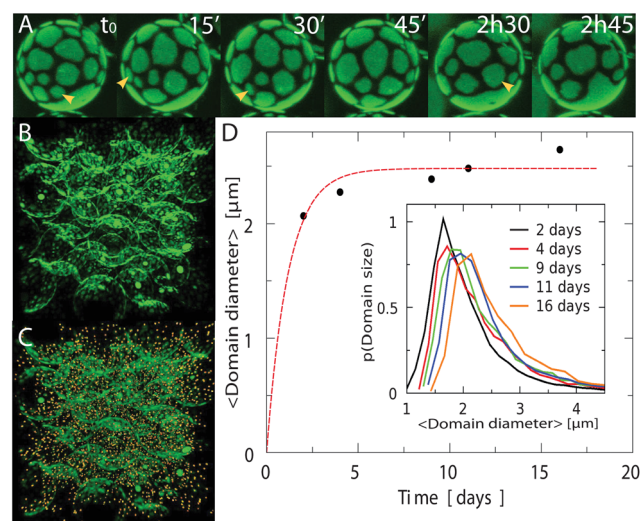


Fig. 5 (A) The domains fluctuate and fuse on the surface of a droplet obtained from a polydisperse emulsion, with the lipid mixture DOPC–Chol 4 : 1. The arrows indicate the domain that is about to fuse in the next image. Droplet diameter = $14\text{ }\mu\text{m}$. (B) A 3D transparent packing of monodisperse droplets (DOPC–Chol 7 : 3) displays bright spots and is imaged through confocal microscopy. (C) Image analysis identifies each patch center, indicated by the orange dots, and radius in the packing. (D) For this lipid composition the bright patches rapidly reach a stable size that doesn't evolve significantly over weeks at room temperature. The corresponding radii distributions are shown in the inset.

minimize liquid–liquid interfaces, while the electrostatic repulsion between the lipid domains keeps them from coalescing.^{60–62} Even though the electrostatic energies are reduced at the oil–water interface,^{63,64} they are strong enough to keep the domains stable on surprisingly long timescales in our system.

3.4 Diffusion of the lipids

The long-lived patches on the emulsion surfaces can be used to assemble larger scale structures through specific patch interactions. The diffusion of the binders within the patches controls the kinetics of the assembly process and should depend on the domain morphologies as shown previously for bilayers.³² We therefore measure the diffusion of streptavidin coated colloids, which are bound to biotinylated phospholipids in the bright liquid-disordered domains. Since the colloid can bind to multiple lipids on the surface, the diffusion constant corresponds to the mobility of the adhered lipids and the viscous drag of the bead on the surface. The colloids are darker than the emulsion droplets and are identified by thresholding, as shown in Fig. 6A. The movement of the colloid on the surface of the droplet is tracked over time to yield the mean square displacement, as shown in Fig. 6B. The linear relationship indicates that the lipids undergo normal diffusion, while the spread of the slopes of the lines shows that the diffusion constant varies slightly from droplet to droplet and more significantly between different droplet morphologies. Homogeneous droplets stabilized by DOPC and biotinylated lipids have the highest diffusion coefficient of $\langle D \rangle = 0.36 \mu\text{m}^2 \text{s}^{-1}$. This value is governed by the viscous drag of the phospholipid tails in the 50 Cst silicone oil phase, in agreement with previous studies.^{65,66} For example, repeating the experiment with a higher viscosity oil of 350 Cst leads to a lower diffusion constant $\langle D \rangle = 0.012 \mu\text{m}^2 \text{s}^{-1}$ in homogeneous droplets. Alternatively, the average diffusion constant is lowered by spatial constraints imposed by the

droplet morphology, as shown in the inset in Fig. 6B. In the case of domains on a bright background the lipids bound to the colloid are free to diffuse inbetween the domains over the entire droplet surface. The presence of obstacles roughly halves the average diffusion constant. Moreover, confining the lipids within the bright spots on a dark background further slows down their diffusion. Finally, when the lipids precipitate into a gel phase the diffusion constant is as low as $\langle D \rangle = 0.0074 \mu\text{m}^2 \text{s}^{-1}$ since the structures exhibit very little motion.

These results are in qualitative agreement with the trends observed in bilayers. The highest diffusion constant of $\approx 13.4 \mu\text{m}^2 \text{s}^{-1}$ is measured in model membranes of pure DOPC, while the introduction of cholesterol reduces it to $\approx 8.9 \mu\text{m}^2 \text{s}^{-1}$.⁶⁷ A more dramatic effect is observed in biological membranes, where the presence of transmembrane proteins, the underlying cytoskeleton and raft-like structures slows down the diffusion of lipids to a range from 0.1 to $1 \mu\text{m}^2 \text{s}^{-1}$ depending on the cell type.^{68,69}

4 Conclusions

We have presented a versatile system of patchy particles for self-assembly, in which the morphology is predicted by the ternary immiscibility phase diagram of lipids. The advantage of this system is that the patch formation is spontaneous and requires no surface modifications or multi-step synthesis. Microfluidic emulsification with a given lipid mixture leads to monodisperse droplets with uniform patch morphologies that are stable over weeks. Another inherent advantage of this system is that the fluidity of the surface adds an extra degree of freedom to the self-assembly process: the system will be able to explore configurations even after droplets bind together through the sticky patches. In this paper, we have quantified the diffusion constant in different droplet morphologies, such that the timescale on which the configurations are sampled can be finely tuned. Bringing together the control of the number of

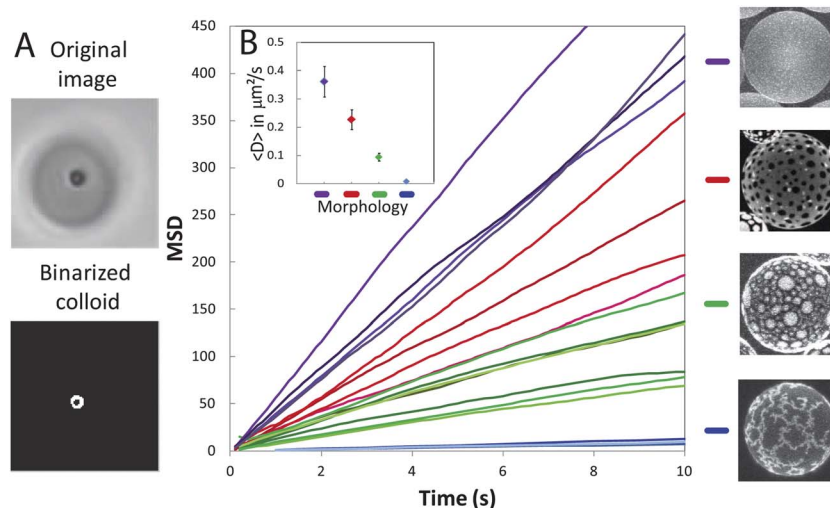


Fig. 6 Raw images show the darker bead diffusing on the surface of the immobile droplet (A). A good contrast allows thresholding of the image to isolate the particle for its tracking (B) and the subsequent diffusion coefficient estimation. The diffusion coefficients were thus obtained for various morphologies and the analysis was performed on different droplets for each condition, grouped by colors in (B). The inset in (B) shows the average values of the diffusion coefficient for each analyzed morphology.

functionalized patches per particle (by tuning the droplet size or lipid composition) and the mobility of the domains (by the viscosity of the oil) opens the path to building super-structures with a programmable design. For example, the emulsion in Fig. 2D has ≈ 6 patches per particle, which may assemble into super-structures with octahedral symmetry if all the patches are bound to each other. Other patch valencies and morphologies are predicted to lead to a wide array of structures.¹⁰

More generally, we have discovered a system of stable domains on curved oil-in-water interfaces of emulsion droplets. Their phase diagram resembles that of other monolayers and reveals long-lived domains of different shapes. One plausible explanation for the stability of domains with a characteristic length scale is an equilibrium balance between line tension around the domains and long-range repulsive forces, such as the dipole-dipole electrostatic repulsion between the domains.^{70,71} This theoretical framework predicts nearly circular domains of a given size on the droplet surface. The experimental size distribution therefore indicates deviations from equilibrium that may be a result of deep kinetic traps along the way. Moreover, it is unclear how the spherical topology of the droplet influences these long range interactions, given that the curved surface introduces a finite length scale compared to flat monolayers.

Depending on the shape of the energy landscape, this equilibrium phase can be reached *via* different kinetic pathways. If a temperature jump leads to an instability, then the system will spontaneously exhibit a spinodal decomposition along the downhill slope towards equilibrium. By contrast, the presence of a barrier imposes a nucleation and growth mechanism for the formation of circular domains. Such a scenario leads to the coalescence of smaller domains with larger ones until a stable domain size is reached. Our experiments reveal examples of both those mechanisms, depending on the composition of the lipids.

Alternatively, if the system is out of equilibrium and there is a reservoir of lipids that remains in the bulk oil, the lipids may be recruited into the domains and thus drive coarsening on timescales that are beyond those probed in the experiment.^{72,73} In that case, the equilibrium state implies complete phase separation. This mechanism does not preclude the kinetic pathways observed in the experiment. Future work will require a more detailed study of the interaction energies involved in the experimental system to distinguish between the possible scenarios for stable domain formation. This technique may therefore be extended to other lipid mixtures, while the phase diagram can be further manipulated by external parameters, such as the temperature, pH and salt concentration. Such studies will shed new light on the mechanisms of domain formation and stabilization.

Acknowledgements

We would like to acknowledge Kenneth Desmond, Lang Feng and Ivane Jorjadze for their help with the experiments and Cyrill Muratov for theoretical insights. This work was supported partially by the MRSEC Program of the National Science

Foundation under Grant no. DMR-0820341 and the National Science Foundation Career Grant no. 0955621.

References

- 1 G. M. Whitesides and B. Grzybowski, Self-assembly at all scales, *Science*, 2002, **295**(5564), 2418–2421.
- 2 J. Lee, P. Hernandez, J. Lee, A. Govorov and N. Kotov, Exciton-plasmon interactions in molecular spring assemblies of nanowires and wavelength-based protein detection, *Nat. Mater.*, 2007, **6**(4), 291–295.
- 3 C. E. Reese, M. E. Baltusavich, J. P. Keim and S. A. Asher, Development of an intelligent polymerized crystalline colloidal array colorimetric reagent, *Anal. Chem.*, 2001, **73**(21), 5038–5042.
- 4 I. I. Tarhan and G. H. Watson, Photonic band structure of fcc colloidal crystals, *Phys. Rev. Lett.*, 1996, **76**, 315–318.
- 5 L. Feng, S. H. Park, J. H. Reif and H. Yan, A two-state DNA lattice switched by DNA nanoactuator, *Angew. Chem.*, 2003, **115**(36), 4478–4482.
- 6 H. J. Schope, T. Decker and T. Palberg, Response of the elastic properties of colloidal crystals to phase transitions and morphological changes, *J. Chem. Phys.*, 1998, **109**(22), 10068–10074.
- 7 F. X. Redl, K.-S. Cho, C. B. Murray and S. O'Brien, Three-dimensional binary superlattices of magnetic nanocrystals and semiconductor quantum dots, *Nature*, 2003, **423**(6943), 968–971.
- 8 J. J. Urban, D. V. Talapin, E. V. Shevchenko, C. R. Kagan and C. B. Murray, Synergism in binary nanocrystal superlattices leads to enhanced p-type conductivity in self-assembled PbTe/Ag₂Te thin films, *Nat. Mater.*, 2007, **6**(2), 115–121.
- 9 D. H. Gracias, M. Boncheva, O. Omoregie and G. M. Whitesides, Biomimetic self-assembly of helical electrical circuits using orthogonal capillary interactions, *Appl. Phys. Lett.*, 2002, **80**(15), 2802–2804.
- 10 Z. Zhang and S. C. Glotzer, Self-assembly of patchy particles, *Nano Lett.*, 2004, **4**(8), 1407–1413.
- 11 A. J. Williamson, A. W. Wilber, J. P. K. Doye and A. A. Louis, Templated self-assembly of patchy particles, *Soft Matter*, 2011, **7**, 3423–3431.
- 12 S. Hormoz and M. P. Brenner, Design principles for self-assembly with short-range interactions, *Proc. Natl. Acad. Sci. U. S. A.*, 2011, **108**(13), 5193–5198.
- 13 A. M. Jackson, J. W. Myerson and F. Stellacci, Spontaneous assembly of subnanometre-ordered domains in the ligand shell of monolayer-protected nanoparticles, *Nat. Mater.*, 2004, **3**(5), 330–336.
- 14 F. Wang, L. Cheng, T. Chen, D. Zhu, Q. Wen and S. Wang, Facile preparation of polymeric dimers from amphiphilic patchy particles, *Macromol. Rapid Commun.*, 2012, **33**(10), 933–937.
- 15 L. Feng, R. Dreyfus, R. Sha, N. C. Seeman and P. M. Chaikin, DNA patchy particles, *Adv. Mater.*, 2013, 2779–2783.
- 16 Z. Tang, Z. Zhang, Y. Wang, S. C. Glotzer and N. A. Kotov, Self-assembly of CdTe nanocrystals into free-floating sheets, *Science*, 2006, **314**(5797), 274–278.

- 17 Z. L. Zhang, Z. Y. Tang, N. A. Kotov and S. C. Glotzer, Simulations and analysis of self-assembly of CdTe nanoparticles into wires and sheets, *Nano Lett.*, 2007, **7**(6), 1670–1675.
- 18 S. Srivastava, A. Santos, K. Critchley, K.-S. Kim, P. Podsiadlo, K. Sun, J. Lee, C. Xu, G. D. Lilly, S. C. Glotzer and N. A. Kotov, Light-controlled self-assembly of semiconductor nanoparticles into twisted ribbons, *Science*, 2010, **327**(5971), 1355–1359.
- 19 L. Rossi, S. Sacanna, W. T. M. Irvine, P. M. Chaikin, D. J. Pine and A. P. Philipse, Cubic crystals from cubic colloids, *Soft Matter*, 2011, **7**, 4139–4142.
- 20 S. Sacanna, W. T. M. Irvine, P. M. Chaikin and D. J. Pine, Lock and key colloids, *Nature*, 2010, **464**(7288), 575–578.
- 21 P. F. Devaux and R. Morris, Transmembrane asymmetry and lateral domains in biological membranes, *Traffic*, 2004, **5**(4), 241–246.
- 22 D. L. Daleke, Phospholipid flippases, *J. Biol. Chem.*, 2007, **282**(2), 821–825.
- 23 D. A. Brown and E. London, Functions of lipid rafts in biological membranes, *Annu. Rev. Cell Dev. Biol.*, 1998, **14**(1), 111–136, PMID: 9891780.
- 24 D. Brown and E. London, Structure and origin of ordered lipid domains in biological membranes, *J. Membr. Biol.*, 1998, **164**, 103–114.
- 25 D. A. Brown and E. London, Structure and function of sphingolipid- and cholesterol-rich membrane rafts, *J. Biol. Chem.*, 2000, **275**(23), 17221–17224.
- 26 K. Jacobson and C. Dietrich, Looking at lipid rafts?, *Trends Cell Biol.*, 1999, **9**(3), 87–91.
- 27 K. Jacobson, E. D. Sheets and R. Simson, Revisiting the fluid mosaic model of membranes, *Science*, 1995, **268**(5216), 1441–1442.
- 28 K. Simons and E. Ikonen, Functional rafts in cell membranes, *Nature*, 1997, **387**, 569–572.
- 29 K. Simons and E. Ikonen, How cells handle cholesterol, *Science*, 2000, **290**(5497), 1721–1726.
- 30 C. Dietrich, L. Bagatolli, Z. Volovyk, N. Thompson, M. Levi, K. Jacobson and E. Gratton, Lipid rafts reconstituted in model membranes, *Biophys. J.*, 2001, **80**(3), 1417–1428.
- 31 C. Yuan, J. Furlong, P. Burgos and L. J. Johnston, The size of lipid rafts: an atomic force microscopy study of ganglioside gm1 domains in sphingomyelin/dopc/cholesterol membranes, *Biophys. J.*, 2002, **82**, 2526–2535.
- 32 N. Kahya, D. Scherfeld, K. Bacia, B. Poolman and P. Schwille, Probing lipid mobility of raft-exhibiting model membranes by fluorescence correlation spectroscopy, *J. Biol. Chem.*, 2003, **278**(30), 28109–28115.
- 33 S. L. Veatch and S. L. Keller, Separation of liquid phases in giant vesicles of ternary mixtures of phospholipids and cholesterol, *Biophys. J.*, 2003, **85**(5), 3074–3083.
- 34 R. F. de Almeida, A. Fedorov and M. Prieto, Sphingomyelin/phosphatidylcholine/cholesterol phase diagram: Boundaries and composition of lipid rafts, *Biophys. J.*, 2003, **85**(4), 2406–2416.
- 35 A. Roux, D. Cuvelier, P. Nassoy, J. Prost, P. Bassereau and B. Goud, Role of curvature and phase transition in lipid sorting and fission of membrane tubules, *EMBO J.*, 2005, **24**(8), 1537–1545.
- 36 J. C. Lawrence, D. E. Saslowsky, J. M. Edwardson and R. M. Henderson, Real-time analysis of the effects of cholesterol on lipid raft behavior using atomic force microscopy, *Biophys. J.*, 2003, **84**(3), 1827–1832.
- 37 S. L. Keller, T. G. Anderson and H. M. McConnell, Miscibility critical pressures in monolayers of ternary lipid mixtures, *Biophys. J.*, 2000, **79**(4), 2033–2042.
- 38 B. L. Stottrup, D. S. Stevens and S. L. Keller, Miscibility of ternary mixtures of phospholipids and cholesterol in monolayers, and application to bilayer systems, *Biophys. J.*, 2005, **88**(1), 269–276.
- 39 B. L. Stottrup and S. L. Keller, Phase behavior of lipid monolayers containing dppc and cholesterol analogs, *Biophys. J.*, 2006, **90**(9), 3176–3183.
- 40 L.-L. Pontani, I. Jorjadze, V. Viasnoff and J. Brujic, Biomimetic emulsions reveal the effect of mechanical forces on cell–cell adhesion, *Proc. Natl. Acad. Sci. U. S. A.*, 2012, 9839–9844.
- 41 A. L. Hiddessen, S. D. Rodgers, D. A. Weitz and D. A. Hammer, Assembly of binary colloidal structures via specific biological adhesion, *Langmuir*, 2000, **16**(25), 9744–9753.
- 42 L. Cohen-Tannoudji, E. Bertrand, J. Baudry, C. Robic, C. Goubault, M. Pellissier, A. Johner, F. Thalmann, N. K. Lee, C. M. Marques and J. Bibette, Measuring the kinetics of biomolecular recognition with magnetic colloids, *Phys. Rev. Lett.*, 2008, **100**, 108301.
- 43 C. A. Mirkin, R. L. Letsinger, R. C. Mucic and J. J. Storhoff, A DNA-based method for rationally assembling nanoparticles into macroscopic materials, *Nature*, 1996, **382**(6592), 607–609.
- 44 M. Hadorn, E. Boenzli, K. T. Sørensen, H. Fellermann, P. Eggenberger Hotz and M. M. Hanczyc, Specific and reversible DNA-directed self-assembly of oil-in-water emulsion droplets, *Proc. Natl. Acad. Sci. U. S. A.*, 2012, **109**(50), 20320–20325.
- 45 A. S. Utada, L.-Y. Chu, A. Fernandez-Nieves, D. R. Link, C. Holtze and D. A. Weitz, Dripping, jetting, drops, and wetting: The magic of microfluidics, *MRS Bull.*, 2007, **32**, 702–708.
- 46 N. Otsu, A threshold selection method from gray-level histograms, *IEEE Trans. Syst. Man Cybern.*, 1979, **9**(1), 62–66.
- 47 S. L. Veatch and S. L. Keller, Miscibility phase diagrams of giant vesicles containing sphingomyelin, *Phys. Rev. Lett.*, 2005, **94**, 148101.
- 48 M. Edidin, The state of lipid rafts: From model membranes to cells, *Annu. Rev. Biophys. Biomol. Struct.*, 2003, **32**(1), 257–283, PMID: 12543707.
- 49 P. Sengupta, A. Hammond, D. Holowka and B. Baird, Structural determinants for partitioning of lipids and proteins between coexisting fluid phases in giant plasma membrane vesicles, *Biochim. Biophys. Acta, Biomembr.*, 2008, **1778**(1), 20–32.
- 50 A. S. Utada, E. Lorceau, D. R. Link, P. D. Kaplan, H. A. Stone and D. A. Weitz, Monodisperse double

- emulsions generated from a microcapillary device, *Science*, 2005, **308**(5721), 537–541.
- 51 D. J. Benvegnu and H. M. McConnell, Surface dipole densities in lipid monolayers, *J. Phys. Chem.*, 1993, **97**(25), 6686–6691.
- 52 C. C. Lai, S. H. Yang and B. J. Finlayson-Pitts, Interactions of monolayers of unsaturated phosphocholines with ozone at the air–water interface, *Langmuir*, 1994, **10**(12), 4637–4644.
- 53 A. Radhakrishnan and H. M. McConnell, Condensed complexes of cholesterol and phospholipids, *Biophys. J.*, 1999, **77**(3), 1507–1517.
- 54 I. C. Pons-Siepermann and S. C. Glotzer, Design of patchy particles using ternary self-assembled monolayers, *Soft Matter*, 2012, **8**, 6226–6231.
- 55 H. Wolf and D. Woermann, Viscous fingering at the liquid/liquid interface between two coexisting phases of mixtures with a miscibility gap, *Berichte der Bunsen-Gesellschaft für Physikalische Chemie*, 1998, **102**(12), 1783–1793.
- 56 A. Arnéodo, Y. Couder, G. Grasseau, V. Hakim and M. Rabaud, Uncovering the analytical Saffman–Taylor finger in unstable viscous fingering and diffusion-limited aggregation, *Phys. Rev. Lett.*, 1989, **63**, 984–987.
- 57 N. Vladimirova, A. Malagoli and R. Mauri, Two-dimensional model of phase segregation in liquid binary mixtures, *Phys. Rev. E: Stat. Phys., Plasmas, Fluids, Relat. Interdiscip. Top.*, 1999, **60**, 6968–6977.
- 58 S. L. Keller and H. M. McConnell, Stripe phases in lipid monolayers near a miscibility critical point, *Phys. Rev. Lett.*, 1999, **82**, 1602–1605.
- 59 Y. Hu, K. Y. C. Lee and J. Israelachvili, Sealed minitrough for microscopy and long-term stability studies of Langmuir monolayers, *Langmuir*, 2003, **19**(1), 100–104.
- 60 H. McConnell, Equilibration rates in lipid monolayers, *Proc. Natl. Acad. Sci. U. S. A.*, 1996, **93**(26), 15001–15003.
- 61 H. M. McConnell, Structures and transitions in lipid monolayers at the air–water interface, *Annu. Rev. Phys. Chem.*, 1991, **42**(1), 171–195.
- 62 R. De Koker and H. M. McConnell, Hydrodynamics of domain size equilibration in monolayers, *J. Phys. Chem. B*, 1998, **102**(35), 6927–6931.
- 63 H. Möhwald, A. Dietrich, C. Böhm, G. Brezesinski and M. Thoma, Domain formation in monolayers, *Mol. Membr. Biol.*, 1995, **12**(1), 29–38.
- 64 M. Thoma and H. Möhwald, Phospholipid monolayers at hydrocarbon/water interfaces, *J. Colloid Interface Sci.*, 1994, **162**(2), 340–349.
- 65 M. Negishi, H. Seto, M. Hase and K. Yoshikawa, How does the mobility of phospholipid molecules at a water/oil interface reflect the viscosity of the surrounding oil?, *Langmuir*, 2008, **24**(16), 8431–8434, PMID: 18646878.
- 66 R. B. Walder, A. Honciuc and D. K. Schwartz, Phospholipid diffusion at the oil/water interface, *J. Phys. Chem. B*, 2010, **114**(35), 11484–11488.
- 67 S. Ladha, A. Mackie, L. Harvey, D. Clark, E. Lea, M. Brullemans and H. Duclouhier, Lateral diffusion in planar lipid bilayers: a fluorescence recovery after photobleaching investigation of its modulation by lipid composition, cholesterol, or alamethicin content and divalent cations, *Biophys. J.*, 1996, **71**(3), 1364–1373.
- 68 J. Schlessinger, D. E. Koppel, D. Axelrod, K. Jacobson, W. W. Webb and E. L. Elson, Lateral transport on cell membranes: mobility of concanavalin a receptors on myoblasts, *Proc. Natl. Acad. Sci. U. S. A.*, 1976, **73**(7), 2409–2413.
- 69 G. M. Lee and K. Jacobson, Chapter 5 lateral mobility of lipids in membranes, in *Cell Lipids vol. 40 of Current Topics in Membranes*, ed. D. Hoekstra, Academic Press, 1994, pp. 111–142.
- 70 C. Sagui and R. C. Desai, Kinetics of phase separation in two-dimensional systems with competing interactions, *Phys. Rev. E: Stat. Phys., Plasmas, Fluids, Relat. Interdiscip. Top.*, 1994, **49**, 2225–2244.
- 71 H. M. McConnell and V. T. Moy, Shapes of finite two-dimensional lipid domains, *J. Phys. Chem.*, 1988, **92**(15), 4520–4525.
- 72 S. C. Glotzer, E. A. Di Marzio and M. Muthukumar, Reaction-controlled morphology of phase-separating mixtures, *Phys. Rev. Lett.*, 1995, **74**, 2034–2037.
- 73 C. Muratov, Droplet phases in non-local ginzburg-landau models with coulomb repulsion in two dimensions, *Commun. Math. Phys.*, 2010, **299**(1), 45–87.